Tensor correlations in ^{4}He and ^{8}Be within an antisymmetrized quasicluster model

H. Matsuno and Y. Kanada-En'yo
Department of Physics, Kyoto University, Kitashirakawa Oiwake-Cho, Kyoto 606-8502, Japan

N. Itagaki
Yukawa Institute for Theoretical Physics, Kyoto University, Kitashirakawa Oiwake-Cho, Kyoto 606-8502, Japan

(Received 28 May 2018; revised manuscript received 20 September 2018; published 13 November 2018)

In this paper, we extend the framework of the improved version of a simplified method to take into account the tensor contribution (iSMT) and propose the AQCM-T, a tensor version of the antisymmetrized quasicluster model (AQCM). Although the AQCM-T is phenomenological, we can treat the ^3S-^3D coupling in the deuteronlike $T = 0$ NN pair induced by the tensor interaction in a very simplified way, which allows us to proceed to heavier nuclei. Using the AQCM-T and the V2m interaction, where the triplet-even channel of the Volkov no. 2 interaction is weakened to 60% so as to reproduce the binding energy of ^{4}He after including the tensor term of a realistic interaction, the significant tensor contribution in ^{4}He is shown, which is almost comparable to the central interaction, where the D state mixes by 8% to the major S state. The AQCM-T with the new interaction is also applied to ^{8}Be. It is found that the tensor suppression gives a significant contribution to the short-range repulsion between two α clusters.

DOI: 10.1103/PhysRevC.98.054306

I. INTRODUCTION

The nucleus ^{4}He is the strongly bound four-nucleon system with large binding energy per nucleon in the light mass region, and α particles called α clusters can be basic building blocks of the nuclear structure. Based on the assumption that nuclear systems are composed of α clusters, α cluster models [1,2] have been developed and applied in numerous works for the description of nuclear structures including the so-called Hoyle state of ^{12}C [3–5]. Describing cluster states is a challenge for the shell models including modern *ab initio* ones [6–8], since quite a large model space is required. Our goal is to pave the way to generally describe the nuclear structure, both cluster and shell structures. In this study, we start with the cluster side and construct a model that can deal with higher correlations, in particular the tensor correlation, in an economic way with less computational efforts.

There have been fundamental discussions for the appearance of cluster structure in the 1960s on why clustering is favored. The appearance could be related to the nature of the meson exchange potential; one-pion exchange potential (OPEP), which is the exchange of isovector mesons, vanishes when each α cluster has isospin $T = 0$ [9]. As a result, the intercluster interaction is weak, and two-pion exchange potential gives almost satisfactory phase shifts of the α-α scattering. Therefore, the appearance of cluster structure is a natural consequence of the meson theory. In OPEP, the tensor term plays a dominant role, thus the clustering can be considered as the embodiment of suppression or screening of the tensor interaction.

The tensor interaction also plays a crucial role inside ^{4}He. It has been already pointed out in *ab initio* calculations in the 1970s that the contribution of two-particle–two-hole $(2p2h)$ states is very important in ^{4}He because of the strong tensor effect [10]. According to the modern *ab initio* calculations, the contribution of the tensor interaction to the ^{4}He binding energy is quite large. For instance, in the case of the AV8′ potential, it is more than 68 MeV and even more important than the central interaction [11]. Therefore, the tensor interaction plays key roles in both mechanisms for the appearance of the clustering: strong binding of each α cluster and weak interaction between the clusters.

It has been pointed out that this strong tensor contribution in ^{4}He can be suppressed when another ^{4}He approaches, due to the Pauli blocking effect [12]. The appearance of the α-α cluster structure in ^{8}Be, which is confirmed by *ab initio* quantum Monte Carlo calculation [13], is also attributed to the tensor suppression effect. In Ref. [12], the Brueckner theory has been introduced to estimate this suppression effect, while keeping each α cluster to a simple $(0s)^4$ configuration. The improvement of this model space has been performed in Ref. [14]; nevertheless, it is quite important to discuss this suppression effect by treating the tensor contribution in a more direct way.

In most of the conventional cluster models, each α cluster is often assumed as a simple $(0s)^4$ configuration placed at some spatial point. In such simple models, since α cluster is a spin singlet object, contributions of noncentral interactions such as the tensor interaction, as well as the spin-orbit interaction, completely vanish, even though they play crucial roles in the nuclear structure. One needs to take into account cluster breaking components to explicitly deal with the noncentral interactions. Recently, many microscopic attempts of directly taking into account the noncentral interactions for the studies of cluster structure have begun. For instance, the methods of antisymmetrized molecular

dynamics (AMD) [15–18] and Fermionic molecular dynamics (FMD) [19–21] combined with the unitary correlation method (UCOM) have been developed and extensively applied. In AMD and FMD, each nucleon is independently treated as a Gaussian wave packet localized in the phase space, which enables us to describe various cluster structures and also the shell-model structure, where clusters are broken. Also, the complex Gaussian centroid of the single-nucleon wave function is suitable for taking into account the noncentral interactions. The tensor effect in ^{4}He has been studied by extended AMD [22]. In UCOM, by unitary transforming the Hamiltonian, the tensor effect is included, which in principle induces many-body operators up to A (mass number) body, thus the truncation of the model space is required. Our strategy is slightly different; although it is phenomenological, we introduce an effective model to directly take into account the noncentral interactions in a simplified manner.

Concerning the inclusion of the rank-1 noncentral interaction, the spin-orbit interaction, in the cluster model, we proposed the antisymmetrized quasicluster model (AQCM) [23–33]. By introducing a parameter for the imaginary part of the Gaussian centroids of α clusters, we can smoothly transform α clusters to jj-coupling shell model wave functions, and the transformed α clusters are called quasiclusters. As it is well known, the conventional α cluster models cover the model space of closure of major shells ($N = 2$, $N = 8$, $N = 20$, etc.), but not subclosure configurations, where the spin-orbit interaction contributes. Our AQCM can be regarded as an extended cluster model that covers also the jj-coupling subclosure configurations.

However the rank-2 noncentral interaction, i.e., the tensor interaction, is more complicated to treat in the cluster model. The tensor interaction has two features: the first order type and the second order type. The first order one is rather weak and characterized by the attractive effect for a proton (neutron) with the j-upper orbit of the jj-coupling shell model and a neutron (proton) with a j-lower orbit [34], which can be included just by switching on the tensor interaction using the AQCM.

For the second order type ($2p2h$ type), which is more difficult to treat in the cluster model, we have proposed a simplified model to directly take into account the tensor contribution (SMT) [35]. We started with the $(0s)^4$ configuration for an α cluster as an unperturbed configuration and expressed deuteronlike excitation of a proton and a neutron to higher shells by shifting the positions of Gaussian centroids of these two particles. However, the resultant tensor contribution was not as large as expected. Shifting the positions of Gaussian centroids could not be sufficient in mixing higher momentum components of the $2p2h$ configurations.

According to the tensor optimized shell model (TOSM) [36–40] and tensor optimized AMD (TOAMD) [41,42] calculations, the p orbits of this $2p2h$ state must have a very shrunken shape compared with the normal shell model orbits, and this means that mixing of very high momentum components is quite important. Then, we further developed an improved version of the SMT, which is the iSMT [43]. In the method, imaginary parts of the Gaussian centroids are shifted. The imaginary part of the Gaussian centroid corresponds to the expectation value of momentum for the nucleon. The tensor interaction has the character which is suited to be described in the momentum space, and this method is more efficient in directly mixing the higher momentum components of $2p2h$ configurations. The contribution of the tensor interaction in ^{4}He was more than -40 MeV—four times larger than the previous version. The method was also applied to ^{16}O, where the tensor contribution is also large, and this is coming from the finite size effect for the distances among α clusters with a tetrahedral configuration. The model space of the iSMT is further extended in high-momentum AMD (HM-AMD) [44,45], and even more tensor contribution was obtained in ^{4}He.

It should be commented that the shifting imaginary parts of the Gaussian centroids has been already achieved in the original AQCM for the spin-orbit force; centroids were shifted so that two neutrons (or two protons) in an α cluster have finite momenta in opposite directions. What is essential in the iSMT is that high momentum component is taken into account by shifting imaginary part for a proton and a neutron with the isospin $T = 0$. In this sense, the iSMT can be regarded as an extended AQCM for the tensor effect.

In this paper, we further develop the iSMT and newly propose the AQCM-T, which is the tensor version of the AQCM introduced by the authors and their collaborators. This is also regarded as a specific version of the HM-AMD developed by Myo *et al.* In the previous analyses based on the iSMT and HM-AMD, the tensor interaction was just added to the (conventional) effective Hamiltonian. Since the tensor effect was already renormalized in the strong triplet-even (^3E) central part of the effective Hamiltonian, it was double counted. Indeed, ^{4}He was too much overbound, different from the realistic one. In this study, we construct a new framework of the AQCM-T and examine an effective interaction with the central and tensor parts, where the triplet-even part of the central interaction is weakened so as to reproduce the binding energy of ^{4}He within the AQCM-T. We analyze internal wave functions of the correlated NN pairs and show the contribution of the tensor correlation in relatively shorter ranges of the ^3D and ^3S channels compared with the uncorrelated $[(0s)^2]$ NN pair. We also apply the method to ^{8}Be and study tensor effects in the two α cluster structure. It is found that the suppression of the tensor correlation significantly contributes to the short-range repulsion of two α clusters.

This paper is organized as follows: In Sec. II, the framework, especially for the model wave function, is explained. In Sec. III, the Hamiltonian of the present model including the new effective interaction is described. In Secs. IV and V, the numerical results for ^{4}He and ^{4}Be are presented, respectively. The summary is presented in Sec. VI. The fitting procedure of the tensor term of a realistic interaction is explained in Appendix A, and the width parameter dependence of the results for ^{4}He is shown in Appendix B.

II. FORMULATIONS

A. AQCM-T for a NN pair

In this article, we introduce a new framework called the AQCM-T. Although all the nucleons can be treated as

independent Gaussians, we take notice of the correlation of two nucleons, which is taken into account by properly setting the Gaussian centroids of the two nucleons. We start the discussion with a single NN pair.

Each single-particle wave function is written by a Gaussian wave packet as

$$\psi_j(i) = \phi_{S_j}(\boldsymbol{r}_i)\chi_j(s_i, \tau_i), \tag{1}$$

$$\phi_{S_j}(\boldsymbol{r}_i) = \left(\frac{2\nu}{\pi}\right)^{3/4} e^{-\nu(\boldsymbol{r}_i - \boldsymbol{S}_j)^2}, \tag{2}$$

where $\boldsymbol{S}_j$ $(j = 1, 2)$ is the Gaussian centroid and χ_j is the spin-isospin wave function. The width parameter ν is set to $\nu = 0.25$ fm^{-2} and fixed for all the cases in the present article.

For the two nucleons in a correlated NN pair, we introduce their Gaussian centroids with complex conjugate values,

$$\boldsymbol{S}_{1,2} = \boldsymbol{R} \pm \frac{i\boldsymbol{K}}{\nu}, \tag{3}$$

where $\boldsymbol{R}$ and $\boldsymbol{K}$ are real vectors, and plus (minus) signs are for $j = 1$ ($j = 2$). These two nucleons in the NN pair are the time reversal states to each other.

Then the spatial part of the NN pair wave function can be rewritten by relative and center-of-mass (cm) wave functions using $\boldsymbol{k} \equiv 2\boldsymbol{K}$ as

$$\phi_{S_1}(\boldsymbol{r}_1)\phi_{S_2}(\boldsymbol{r}_2) = \varphi_{\boldsymbol{k}}(\boldsymbol{r})\phi_g(\boldsymbol{r}_g), \tag{4}$$

$$\varphi_{\boldsymbol{k}}(\boldsymbol{r}) = \left(\frac{\nu}{\pi}\right)^{3/4} e^{-(\nu/2)r^2 + i\boldsymbol{k}\cdot\boldsymbol{r} + k^2/2\nu}, \tag{5}$$

$$\phi_g(\boldsymbol{r}_g) = \left(\frac{4\nu}{\pi}\right)^{3/4} e^{-2\nu(\boldsymbol{r}_g - \boldsymbol{R})^2}, \tag{6}$$

where $\boldsymbol{r} = \boldsymbol{r}_1 - \boldsymbol{r}_2$ and $\boldsymbol{r}_g = (\boldsymbol{r}_1 + \boldsymbol{r}_2)/2$ are the relative and cm coordinates of the NN pair, respectively. The expectation values of the coordinates and momenta are given as

$$\langle \boldsymbol{r} \rangle = 0, \quad \langle \boldsymbol{p} \rangle = \boldsymbol{k}, \tag{7}$$

$$\langle \boldsymbol{r}_g \rangle = \boldsymbol{R}, \quad \langle \boldsymbol{p}_g \rangle = 0. \tag{8}$$

Here, $\boldsymbol{p} = (\boldsymbol{p}_1 - \boldsymbol{p}_2)/2$ and $\boldsymbol{p}_g = \boldsymbol{p}_1 + \boldsymbol{p}_2$ are the relative and cm momenta of the NN pair. It should be noted that the Fourier components of the relative wave function $\varphi_{\boldsymbol{k}}(\boldsymbol{r})$ also have a Gaussian form, which is localized at $\boldsymbol{k}$ with the dispersion of ν.

As pointed out by Myo *et al.*, the relative wave function $\varphi_{\boldsymbol{k}}(\boldsymbol{r})$ has the angler dependence coming from the factor $e^{i\boldsymbol{k}\cdot\boldsymbol{r}}$ and contains not only S-wave but higher partial-wave components as

$$e^{i\boldsymbol{k}\cdot\boldsymbol{r}} = 4\pi \sum_{lm} i^l j_l(kr) Y_{lm}(\boldsymbol{e}_k) Y_{lm}(\boldsymbol{e}_r). \tag{9}$$

For the inclusion of the tensor correlation, the ^3D component in the $T = 0$ NN pair, which couples to the ^3S component, is essential. Therefore, we project the NN pair state on the positive-parity state. Suppose that $\boldsymbol{k}$ is set along the z axis as $\boldsymbol{k} = (0, 0, k)$; the positive-parity state φ_k^+ projected from $\varphi_{\boldsymbol{k}}$ is expanded with the l-even basis states as

$$\begin{aligned}\varphi_k^+(\boldsymbol{r}) &= \left(\frac{\nu}{\pi}\right)^{3/4} e^{-(\nu/2)r^2 + k^2/2\nu} \cos(kz) \\ &= \left(\frac{\nu}{\pi}\right)^{3/4} e^{-(\nu/2)r^2 + k^2/2\nu} 4\pi \\ &\quad \times \sum_{l=\text{even}} \sqrt{\frac{2l+1}{4\pi}} i^l j_l(kr) Y_{l0}(\boldsymbol{e}_r), \\ &= \sum_{l=\text{even}} a_l \varphi_k^{(l)}(r) Y_{l0}(\boldsymbol{e}_r),\end{aligned} \tag{10}$$

where a_l is the normalization factor, and $\varphi_k^{(l)}(r)$ is the normalized radial wave function of the l-even basis state and is proportional to $e^{-(\nu/2)r^2} j_l(kr)$.

B. AQCM-T for ^{4}He

Next, the NN pair wave function introduced in the previous subsection is applied to the two nucleons in ^{4}He.

1. *Model wave function of* ^{4}He

For the ^{4}He system, in addition to the correlated NN pair introduced in the previous subsection, we consider a $(0s)^2$ (uncorrelated) pair, and both pairs are placed at the origin. The AQCM-T wave function for ^{4}He is expressed as

$$\begin{aligned}\Phi^{\text{AQCM-T}}_{^4\text{He},0^+} &= \hat{P}^{0+}\mathcal{A}\{\phi_{i\boldsymbol{K}/\nu}\chi_1, \phi_{-i\boldsymbol{K}/\nu}\chi_2, \phi_0\chi_3, \phi_0\chi_4\} \\ &= \hat{P}^{0+}\mathcal{A}\{\phi_{i\boldsymbol{K}/\nu}\phi_{-i\boldsymbol{K}/\nu}\phi_0\phi_0 \otimes \chi_1\chi_2\chi_3\chi_4\},\end{aligned} \tag{11}$$

where $\mathcal{A}$ is the antisymmetrizer, $\hat{P}^{0+}$ is the projection operator to $J^\pi = 0^+$ (in practice numerically performed), and $\phi_0 = \phi_{S=0}$ is the spatial wave function for a nucleon in the $0s$ orbit. The spatial wave function of the total system in the intrinsic frame before the projections is rewritten as

$$\phi_{i\boldsymbol{K}/\nu}\phi_{-i\boldsymbol{K}/\nu}\phi_0\phi_0 = \phi_g(\boldsymbol{r}_g)\phi_g(\boldsymbol{r}'_g)\varphi_{\boldsymbol{k}}(\boldsymbol{r})\varphi_0(\boldsymbol{r}'), \tag{12}$$

$$\boldsymbol{r}_g = \frac{\boldsymbol{r}_1 + \boldsymbol{r}_2}{2}, \quad \boldsymbol{r}'_g = \frac{\boldsymbol{r}_3 + \boldsymbol{r}_4}{2}, \tag{13}$$

$$\boldsymbol{r} = \boldsymbol{r}_1 - \boldsymbol{r}_2, \quad \boldsymbol{r}' = \boldsymbol{r}_3 - \boldsymbol{r}_4. \tag{14}$$

This means that the NN correlation is taken into account through $\varphi_{\boldsymbol{k}}(\boldsymbol{r})$ of the correlated pair.

The AQCM-T wave function for ^{4}He in Eq. (11) is a general expression, which contains basis wave functions used in the preceding works by Itagaki *et al.* [43] and Myo *et al.* [44]. In Ref. [43], the orientation of the vector $\boldsymbol{k}$ was introduced along the z axis, which is the axis of the spin quantization, and in Ref. [44], basis states with $\boldsymbol{k}$ direction perpendicular to the z axis were further introduced, while keeping the spin orientations to the original z and $-z$ directions. In principle, if we prepare spin configurations properly, the orientation of the vector $\boldsymbol{k}$ can be arbitrarily chosen, because the intrinsic wave function is projected to the physical ^{4}He state with $J = 0$. In the present model space, we choose the parameter $\boldsymbol{k}$ as $\boldsymbol{k} = (0, 0, k)$ and consider the important spin and isospin configurations properly. The present choice of the z direction is the same as that in Ref. [43], and this is convenient when

extending the method to heavier systems such as ^{8}Be, because ^{4}He is an axial symmetric object in the intrinsic frame.

One should care about the redundancies originating from the parity and angular momentum projections as well as the Fermi statistics (antisymmetrization). In this model, we take into account all the spin and isospin configurations necessary to express 0^+ states and avoid the redundancy. As a result, for a given k value, the model space for 0^+ states of ^{4}He contains five independent spin and isospin configurations;

$$\chi_1\chi_2\chi_3\chi_4 = \{p\uparrow p\downarrow n\uparrow n\downarrow,\ \ n\uparrow n\downarrow p\uparrow p\downarrow,\ \ p\uparrow n\uparrow p\downarrow n\downarrow,\ \ p\uparrow n\downarrow p\uparrow n\downarrow,\ \ p\uparrow n\downarrow p\downarrow n\uparrow\}. \quad (15)$$

Owing to the projection to $J^\pi = 0^+$, $\Phi^{\text{AQCM-T}}_{^4\text{He},0^+}$ contains only the S-wave ($\varphi_k^{(0)}$) and D-wave ($\varphi_k^{(2)}$) components, which are coupled with the total intrinsic spin $S = 0$ and $S = 2$ of four nucleons, respectively. Here $\varphi_k^{(l)}$ stands for the l-wave relative wave function for the NN pair in the partial wave expansion of Eq. (10). Note that $\varphi^{(0)}_{k=0}$ expresses the uncorrelated NN pair with the $(0s)^2$ configuration.

When we ignore small breaking of the isospin symmetry by the Coulomb interaction, the five configurations in Eq. (15) can be reduced into three channels with respect to spin and isospin symmetries of the NN pair as

$$^1S : \phi_g(\boldsymbol{r}_g)\phi_g(\boldsymbol{r}'_g) \otimes \varphi_k^{(0)}(r)\varphi_0^{(0)}(r') \otimes Y_{00}(\boldsymbol{e}_r)Y_{00}(\boldsymbol{e}_{r'}) \otimes \chi_0^\sigma\chi_0^\sigma \otimes \left[\chi_1^\tau\chi_1^\tau\right]_{T=0}, \quad (16)$$

$$^3S : \phi_g(\boldsymbol{r}_g)\phi_g(\boldsymbol{r}'_g) \otimes \varphi_k^{(0)}(r)\varphi_0^{(0)}(r') \otimes Y_{00}(\boldsymbol{e}_r)Y_{00}(\boldsymbol{e}_{r'}) \otimes \left[\chi_1^\sigma\chi_1^\sigma\right]_{S=0} \otimes \chi_0^\tau\chi_0^\tau, \quad (17)$$

$$^3D : \phi_g(\boldsymbol{r}_g)\phi_g(\boldsymbol{r}'_g) \otimes \varphi_k^{(2)}(r)\varphi_0^{(0)}(r') \otimes \left[Y_{20}(\boldsymbol{e}_r)Y_{00}(\boldsymbol{e}_{r'})\right] \otimes \left[\chi_1^\sigma\chi_1^\sigma\right]_{S=2}]_{J=0} \otimes \chi_0^\tau\chi_0^\tau, \quad (18)$$

where χ_S^σ (χ_T^τ) is the spin (isospin) function of the NN pairs coupled to the spin S (isospin T) state. The first (second) configuration in (16) [(17)] takes into account the NN correlation in the ^1S (^3S) channel. In principle, the short-range correlation caused by the repulsive hard core contributes in these channels, and amplitudes of two nucleons close to each other should be suppressed; however, the central interaction adopted in the present study is not a realistic nuclear force but an effective interaction without a hard core. The third configuration is the so-called D-state component, which is essential in the tensor correlation. We call the first, second, and third configurations, the ^1S, ^3S, and ^3D channels, respectively.

In the present framework, $\Phi^{\text{AQCM-T}}_{^4\text{He},0^+}$ defined in Eqs. (11) and (12) is a basis wave function specified by the k value in Eq. (5) and the spin-isospin configuration. The total wave function for the ground state, $\Psi_{^4\text{He,gs}}$, is expressed by linear combination of various k values and the spin and isospin configurations as

$$\Psi_{^4\text{He,gs}} = c_0\Phi^{0s}_{^4\text{He}} + \sum_k\sum_\beta c(k,\beta)\Phi^{\text{AQCM-T}}_{^4\text{He},0^+}(k,\beta), \quad (19)$$

where β is the label for the spin-isospin configurations in Eq. (15) [or channels in (16)–(18)]. Here, the first term of $\Phi^{0s}_{^4\text{He}}$ is the $(0s)^4$ wave function equivalent to $\Phi^{\text{AQCM-T}}_{^4\text{He},0^+}(k,\beta)$ with $k = 0$ and $\beta = p\uparrow p\downarrow n\uparrow n\downarrow$. The coefficients c_0 and $c(k,\beta)$ are determined by diagonalizing the norm and Hamiltonian matrices comprised of the basis wave functions. The superposition with respect to k in Eq. (19) is nothing but the expansion of the correlated NN pair wave function in terms of Gaussians with mean momentum $\boldsymbol{k}$ in the momentum space, and the sum of β corresponds to the coupled-channel calculation of $\beta = \{^1S, ^3S, \text{and } ^3D\}$.

In the present framework, we take notice of a single NN pair among the four nucleons and explicitly treat the two-body correlations, but we omit higher-order correlations, where more than two nucleons are involved. This ansatz is supported by the four-body calculations by Horii *et al.* in Ref. [46], which demonstrates that the D state coupling with the S state, which is dominant, in a single NN pair with $T = 0$ is essential in describing the ^{4}He ground state. This is a natural consequence of the bosonic feature of two NN pairs with $T = 0$ in ^{4}He.

In this article, we present a new framework and call it the "AQCM-T," because this is a tensor version of the AQCM, in which clusters are changed into quasiclusters characterized by the complex Gaussian centroids. The AQCM has been originally proposed to describe the breaking of nn and α clusters by the spin-orbit interaction at the nuclear surface, and this can be regarded as an extended version of the Brink cluster model or a specific version of the AMD model. The AQCM treatment of introducing the imaginary part for the Gaussian centroids has been applied to a pn pair to describe the tensor correlation in ^{4}He by Itagaki and Tohsaki in Ref. [43], in which the method was called the "iSMT." The model space of the iSMT was extended in "HM-AMD" by Myo *et al.* for the study of the tensor correlations of ^{4}He in Ref. [44]. In order to treat short-range correlations as well as the tensor correlations, they have achieved further extension of the HM-AMD model by taking into account higher-order correlations beyond two body [45]. Our parameter $\boldsymbol{k}$ in Eq. (5) for the imaginary centroids of the Gaussian wave packets is related to the notations of the parameters $\boldsymbol{d}$ in the iSMT and $\boldsymbol{D}$ in HM-AMD as $\boldsymbol{d} = \boldsymbol{D} = \boldsymbol{K}/\nu = \boldsymbol{k}/(2\nu)$. It should be commented that the model spaces of Refs. [43,44] correspond to subsets of the present spin and isospin configurations defined in Eq. (15). One of the key points of the present model is that we explicitly represent not only the isospin symmetry of the correlated pair but also that of the $(0s)^2$ pair, which is essential in describing the isoscalar property of the ^{4}He ground state.

2. *Parameter settings for* ^{4}He

For the ground state of ^{4}He ($^4\text{He}_{\text{gs}}$), we perform calculations with the three channels defined in (16)–(18) ($\beta = \{^1S, ^3S, ^3D\}$). This three-channel calculation can be practically done using five configurations defined in Eq. (15). If we can omit the effect of the charge symmetry breaking by the Coulomb interaction, these two sets of configurations are equivalent. Indeed, the three-channel calculation gives almost the same result as that of the full five configurations, indicating that the symmetry breaking in the isospin space is negligibly small. For each channel, the basis states with $k = 0.5, 1.0, \ldots, 5.5$ fm^{-1} (11 points) are adopted in addition

to the $(0s)^4$ configuration. As a result, the total number of the basis states in Eq. (19) is $11 \times 3 + 1 = 34$ corresponding to the dimension of the Hamiltonian to be diagonalized. We also perform calculations with truncated model space and compare with the full result to clarify the roles of the ^1S, ^3S, and ^3D components.

C. AQCM-T for ^{8}Be

1. AQCM-T wave function of 2α

Our aim is to investigate the tensor effect in heavier nuclei. Here we extend the AQCM-T framework to ^{8}Be with the two α cluster structure, in which one of the α clusters is changed from the $(0s)^4$ configuration to the correlated ^{4}He wave function previously explained. We label the correlated α cluster as α_k, and another α cluster with the $(0s)^4$ configuration is labeled as α_0. We place α_k at $\boldsymbol{R} = \frac{\boldsymbol{d}_\alpha}{2}$ and α_0 at $\boldsymbol{R}' = -\frac{\boldsymbol{d}_\alpha}{2}$ with the relative distance of $\boldsymbol{d}_\alpha$. After the antisymmetrization, the 0^+ projected 2α wave function is

$$\Phi^{\text{AQCM-T}}_{2\alpha,0^+}(k,\beta,\boldsymbol{d}_\alpha) = \hat{P}^{0+}\mathcal{A}\{\Phi_{\alpha_k}(k,\beta,\boldsymbol{R})\Phi_{\alpha_0}(\boldsymbol{R}')\}, \quad (20)$$

where β is the label for the spin and isospin configurations of the α_k cluster. The two α clusters are expressed using the AQCM-T wave function for ^{4}He as

$$\begin{aligned}\Phi_{\alpha_k}(k,\beta,\boldsymbol{R}) &= \Phi^{\text{AQCM-T}}_{^4\text{He},+}(k,\beta,\boldsymbol{R}) \\ &= \frac{1+\hat{P}_k}{2}\mathcal{A}\{\phi_{\boldsymbol{R}+i\boldsymbol{K}/\nu}\phi_{\boldsymbol{R}-i\boldsymbol{K}/\nu}\phi_{\boldsymbol{R}}\phi_{\boldsymbol{R}} \\ &\quad \otimes\chi_1\chi_2\chi_3\chi_4\}, \quad (21)\\ \Phi_{\alpha_0}(\boldsymbol{R}') &= \Phi^{0s}_{^4\text{He}}(\boldsymbol{R}') \\ &= \mathcal{A}\{\phi_{\boldsymbol{R}'}\phi_{\boldsymbol{R}'}\phi_{\boldsymbol{R}'}\phi_{\boldsymbol{R}'}\otimes p\uparrow p\downarrow n\uparrow n\downarrow\}. \quad (22)\end{aligned}$$

Here $\boldsymbol{K} = (0,0,k/2)$, and the operator $\hat{P}_k$ transforms the imaginary part of the correlated NN pair as $k \to -k$. Thus, the intrinsic wave function of the correlated NN pair is projected onto the positive-parity state by the operator $(1+\hat{P}_k)/2$. The parameter $\boldsymbol{d}_\alpha$ for the relative distance is chosen as $\boldsymbol{d}_\alpha = (d_\alpha \sin\theta_\alpha, 0, d_\alpha\cos\theta_\alpha)$. For fixed d_α, states with various k, θ_α, and β values are superposed as

$$\begin{aligned}&\Psi_{2\alpha,0^+}(d_\alpha) \\ &= c_0\Phi^{\text{BB}}_{2\alpha,0^+}(d_\alpha) + \sum_{k,\beta,\theta_\alpha} c(k,\beta,\theta_\alpha)\Phi^{\text{AQCM-T}}_{2\alpha,0^+}(k,\beta,\boldsymbol{d}_\alpha),\end{aligned} \quad (23)$$

where $\Phi^{\text{BB}}_{2\alpha,0^+}$ is the Brink-Bloch (BB) 2α cluster wave function projected to 0^+,

$$\Phi^{\text{BB}}_{2\alpha,0^+}(d_\alpha) = \hat{P}^{0+}\mathcal{A}\{\Phi_{\alpha_0}(\boldsymbol{R})\Phi_{\alpha_0}(\boldsymbol{R}')\}. \quad (24)$$

For each d_α value, the coefficients c_0 and $c(k,\beta,\theta_\alpha)$ are determined by diagonalizing the norm and Hamiltonian matrices. We investigate the tensor correlations of the two α system as a function of d_α.

In the present framework, not only for the relative motion between clusters, the angular momentum of the subsystem α_k is practically projected; although the projection in $\Psi_{2\alpha,0^+}(d_\alpha)$ is only for the total angular momentum, the double projection is achieved. This is owing to the rotational symmetry of the α_0 cluster, the axial symmetry of the α_k, and the superposition effect of states with various θ_α values $(0 \leqslant \theta_\alpha \leqslant \pi/2)$. The range of $\pi/2 \leqslant \theta_\alpha \leqslant \pi$ is redundant in the present case since the intrinsic parity of the α_k cluster is already projected.

Here the angle θ_α is treated as a generator coordinate, while the parameter d_α is fixed, and the intercluster wave function is localized around d_α. In principle, d_α can be also treated as a generator coordinate; superposing $\Psi_{2\alpha,0^+}(d_\alpha)$ with different d_α values gives a better solution for the intercluster motion. However, such calculation requires huge computational costs, and we perform our calculation for each fixed d_α value.

In the present AQCM-T framework for the two α system, we explicitly treat the NN correlation in one of the two α clusters, but we omit configurations that NN pairs in both α clusters are simultaneously excited from $(0s)^2$, which could significantly contribute in the asymptotic region $(d_\alpha \to \infty)$. If each $^4\text{He}_{\text{gs}}$ cluster contains the $(0s)^4$ component $(|0s\rangle)$ still dominantly and the mixing of the correlated component $(|\text{corr}\rangle)$ is minor in amplitude as $|^4\text{He}_{\text{gs}}\rangle \propto |0s\rangle + \varepsilon|\text{corr}\rangle$ with small enough $|\varepsilon|$, the present ansatz is a good approximation; the 2α state at $\boldsymbol{R}$ and $\boldsymbol{R}'$ is written as $|^4\text{He}_{\text{gs}}\rangle_{\boldsymbol{R}}|^4\text{He}_{\text{gs}}\rangle_{\boldsymbol{R}'} = |0s\rangle_{\boldsymbol{R}}|0s\rangle_{\boldsymbol{R}'} + \varepsilon|0s\rangle_{\boldsymbol{R}}|\text{corr}\rangle_{\boldsymbol{R}'} + \varepsilon|\text{corr}\rangle_{\boldsymbol{R}}|0s\rangle_{\boldsymbol{R}'} + \mathcal{O}(\varepsilon^2)$, which can be approximately described by the present model space within the order of $\mathcal{O}(\varepsilon)$. Note that the exchange of the α positions, $\boldsymbol{R} \leftrightarrow \boldsymbol{R}'$, is implicitly performed in the present model by the parity projection of the total system using α clusters, whose intrinsic parities are already projected.

2. Parameter setting for ^{8}Be

For the generator coordinate θ_α for the angle, we adopt five mesh points of $\theta_\alpha = 0, \pi/8, \ldots, \pi/2$, which gives almost converged results. Regarding the correlated α cluster (α_k) wave function, we truncate the configurations introduced for ^{4}He in order to save the computational costs; here we employ only two channels of $\beta = \{^3S, ^3D\}$, because the ^1S channel is found to be not essential for the tensor correlations in ^{4}He as we discuss later. The calculation with these two channels is practically performed by employing the following three configurations:

$$\chi_1\chi_2\chi_3\chi_4 = \{p\uparrow n\uparrow p\downarrow n\downarrow,\ \ p\uparrow n\downarrow p\uparrow n\downarrow,\ \ p\uparrow n\downarrow p\downarrow n\uparrow\}.$$

For the parameter k in Eq. (20), we use three points $k = \{1,2,3\}$ fm^{-1}, which efficiently describes the properties of $^4\text{He}_{\text{gs}}$. Therefore, the number of the basis states in Eq. (23) corresponding to the dimension of the diagonalization is $3 \times 2 \times 5 + 1 = 31$ for a given distance of d_α.

D. 0s, ^1S, ^3S, and ^3D probabilities

In this study, we analyze the probabilities of the ^1S, ^3S, ^3D components in the obtained ^{4}He and two α states $(|\Psi\rangle)$,

$$\mathcal{P}_{^1S,^3S,^3D} = |\langle\Psi|\hat{P}_{^1S,^3S,^3D}|\Psi\rangle|, \quad (25)$$

and the $0s$ probability is given as

$$\mathcal{P}_{0s} = |\langle 0s|\Psi\rangle|^2. \tag{26}$$

Here $|\Psi\rangle = |\Psi_{^4\mathrm{He,gs}}\rangle$ and $|0s\rangle = |\Phi^{0s}_{^4\mathrm{He}}\rangle$ for the ^{4}He system, and $|\Psi\rangle = |\Psi_{2\alpha,0^+}\rangle$ and $|0s\rangle = |\Phi^{\mathrm{BB}}_{2\alpha,0^+}\rangle$ for the two α system. $\hat{P}_{^1S,^3S,^3D}$ are the projection operators onto the ^1S, ^3S, ^3D components. We also calculate the probabilities

$$\mathcal{P}^{\perp}_{^1S,^3S} = |\langle\Psi|\Lambda^{\perp}_{0s}\hat{P}_{^1S,^3S}\Lambda^{\perp}_{0s}|\Psi\rangle|, \tag{27}$$

$$\Lambda^{\perp}_{0s} = 1 - |0s\rangle\langle 0s|, \tag{28}$$

of the correlated ^1S, ^3S components, which are defined in the $\Lambda^{\perp}_{0s}$-projected space orthogonal to the $0s$ state. Note that $\mathcal{P}^{\perp}_{^1S,^3S}$ somewhat depends on the adopted width parameter ν of the Gaussian wave packet defined in Eq. (2) and therefore one should be careful in quantitative discussions on the absolute values of $\mathcal{P}^{\perp}_{^1S,^3S}$.

III. HAMILTONIAN

The Hamiltonian used in the present calculation is

$$\hat{H} = \sum_{i}^{A}\hat{T}_i - \hat{T}_{\mathrm{G}} + \sum_{i<j}^{A}[\hat{V}_{\mathrm{c}}(i,j) + \hat{V}_{\mathrm{so}}(i,j) + \hat{V}_{\mathrm{t}}(i,j) + \hat{V}_{\mathrm{Coulomb}}(i,j)], \tag{29}$$

where $\hat{T}_i$ is the kinetic energy operator of ith nucleon, and the total kinetic energy operator for the cm motion ($\hat{T}_{\mathrm{G}}$) is subtracted. The two-body interaction consists of central interaction ($\hat{V}_{\mathrm{c}}$), spin-orbit interaction ($\hat{V}_{\mathrm{so}}$), tensor interaction ($\hat{V}_{\mathrm{t}}$), and Coulomb interaction ($\hat{V}_{\mathrm{Coulomb}}$) terms. The Coulomb interaction for the protons is approximated by a seven-range Gaussian form.

A. Central interaction

For the central interaction $\hat{V}_{\mathrm{c}}$, we use an effective nucleon-nucleon interaction. Our central interaction is based on the Volkov no. 2 interaction [47], which is a phenomenological one and reproduces the α-α scattering phase shift when the Majorana exchange parameter is properly chosen. The original Volkov interaction has only the Wigner and Majorana exchange terms, but here we add the Bartlett and Heisenberg terms as

$$\hat{V}_{\mathrm{c}} = \left[V_\alpha \exp\left(-\frac{r_{ij}^2}{\alpha^2}\right) + V_\rho \exp\left(-\frac{r_{ij}^2}{\rho^2}\right)\right] \times \left[w + b\hat{P}^{\sigma}_{ij} - h\hat{P}^{\tau}_{ij} - m\hat{P}^{\sigma}_{ij}\hat{P}^{\tau}_{ij}\right], \tag{30}$$

where $V_\alpha = -60.65$ MeV, $V_\rho = 61.14$ MeV, $\alpha = 1.80$ fm, and $\rho = 1.01$ fm, which are the original values.

This is a phenomenological interaction, and tensor effect as well as the hard-core contribution is effectively renormalized in the central interaction, and if we just add the tensor interaction to the Volkov interaction, the tensor effect is double counted. As explained in Sec. III D, we examine the case of an effective interaction containing the central and tensor interaction terms by modifying the original Volkov no. 2 interaction.

B. Spin-orbit interaction

For the spin-orbit interaction $\hat{V}_{\mathrm{so}}$, we use the spin-orbit part of the G3RS interaction [48], which is a realistic nucleon-nucleon interaction, given by

$$\hat{V}_{\mathrm{so}} = \left[u_1 \exp\left(-\frac{r_{ij}^2}{\eta_1^2}\right) + u_2 \exp\left(-\frac{r_{ij}^2}{\eta_2^2}\right)\right]\hat{P}_{ij}(^3O)\hat{\boldsymbol{L}}_{ij}\cdot\hat{\boldsymbol{S}}_{ij}, \tag{31}$$

where $u_1 = 600$ MeV, $u_2 = -1050$ MeV, $\eta_1 = 0.447$ fm, and $\eta_2 = 0.6$ fm which are the values of "case 1" of G3RS. Here $\hat{P}_{ij}(^3O)$ is the projection operator to the triplet odd (^3O) state.

C. Tensor interaction

For the tensor interaction $\hat{V}_{\mathrm{t}}$, we consider a r^2-weighted Gaussian form for the r dependence, which is for the convenience of the practical AQCM-T calculation. Our final goal is to apply the AQCM-T to systems heavier than ^{4}He, and therefore, we here prepare a new parametrization of the r^2-weighted Gaussian with three ranges by fitting the tensor part of G3RS [48], which is a realistic interaction and its spin-orbit part was explained in the previous subsection. The tensor term with the r^2-weighted Gaussian form has been proposed by Furutani *et al.* in the $3N + N$ cluster model calculation for the $A = 4$ system [49] and used for the study of the tensor effect in ^{4}He with an extended AMD by Doté *et al.* [22]. Since Furutani's tensor interaction (called simply Furutani tensor interaction) was tuned for simple wave function, it gives too strong attraction for more sophisticated wave functions containing tensor correlations of NN pairs as shown in Ref. [44], and therefore it is not suitable for the study of the tensor correlation in the realistic ^{4}He. In the present paper, we adopt the same form as the Furutani tensor interaction but tune coefficient of each range so as to reasonably simulate the G3RS tensor interaction. This parametrization is the default tensor part in the AQCM-T calculations for ^{4}He and ^{8}Be. We also show some results of ^{4}He for cases of the original G3RS and Furutani tensor parts just for comparison. Below we present functional forms of the G3RS and Furutani's and our tensor interactions.

The tensor part of G3RS is given by

$$\hat{V}_{\mathrm{t}}^{(\mathrm{G3RS})} = \hat{S}_{ij}\left[\sum_{n=1}^{3} V_{\mathrm{t},n}^{(\mathrm{G3RS})^3E}\hat{P}_{ij}(^3E)\exp\left(-\frac{r_{ij}^2}{\eta_{\mathrm{t},n}^2}\right) + \sum_{n=1}^{3} V_{\mathrm{t},n}^{(\mathrm{G3RS})^3O}\hat{P}_{ij}(^3O)\exp\left(-\frac{r_{ij}^2}{\eta_{\mathrm{t},n}^2}\right)\right], \tag{32}$$

$$\hat{S}_{ij} = 3(\hat{\boldsymbol{\sigma}}_i\cdot\hat{\boldsymbol{r}}_{ij})(\hat{\boldsymbol{\sigma}}_j\cdot\hat{\boldsymbol{r}}_{ij})/r_{ij}^2 - (\hat{\boldsymbol{\sigma}}_i\cdot\hat{\boldsymbol{\sigma}}_j), \tag{33}$$

where $\hat{P}_{ij}(^3E)$ is the projection operator to the triplet even (^3E) state. We use the parameter set of "case 1" of G3RS.

TABLE I. The parameter sets of G3RS tensor part (case 1), Furutani tensor, and new three-range fit (3R fit) tensor, which is G3RS tensor part fitted by using the functional form of the Furutani tensor defined in Eqs. (33)–(35).

n	1	2	3
G3RS tensor part (case 1)			
$\eta_{t,n}$ (fm)	2.5	1.2	0.447
$V_{t,n}^{(\mathrm{G3RS})^3E}$ (MeV)	−7.5	−67.5	67.5
$V_{t,n}^{(\mathrm{G3RS})^3O}$ (MeV)	2.5	20	−20
Furutani tensor			
β_n (fm^{-2})	0.53	1.92	8.95
$V_{t,n}^{(\mathrm{Furutani})}$ (MeV fm^{-2})	−16.96	−369.5	1688.0
W_n	0.3277	0.4102	0.5
H_n	0.6723	0.5898	0.5
New three-range fit tensor			
β_n (fm^{-2})	0.53	1.92	8.95
$V_{t,n}^{(\mathrm{3R\text{-}fit})^3E}$ (MeV fm^{-2})	−17.02	−209.89	−289.59
$V_{t,n}^{(\mathrm{3R\text{-}fit})^3O}$ (MeV fm^{-2})	5.27	62.91	89.87

Furutani tensor interaction is given by

$$\hat{V}_t^{(\mathrm{Furutani})} = \hat{S}_{ij} \sum_{n=1}^{3} V_{t,n}^{(\mathrm{Furutani})} \left(W_n - H_n \hat{P}_{ij}^{\tau}\right) r_{ij}^2 \exp\left(-\beta_n r_{ij}^2\right). \tag{34}$$

This interaction was used in our previous SMT and *i*SMT works. Compared with the Gaussian form of the G3RS tensor part, the Furutani tensor has the r^2-weighted Gaussian form, which allows us to calculate the matrix element easily, when the local Gaussian type of the wave function is introduced as in the present case.

Our newly prepared tensor interaction is given by the r^2-weighted Gaussian form with the same ranges as the Furutani tensor interaction as

$$\hat{V}_t^{(\mathrm{3R\text{-}fit})} = \hat{S}_{ij} \left[\sum_{n=1}^{n_{\max}=3} V_{t,n}^{(\mathrm{3R\text{-}fit})^3E} \hat{P}_{ij}(^3E) r_{ij}^2 \exp\left(-\beta_n r_{ij}^2\right) + \sum_{n=1}^{n_{\max}=3} V_{t,n}^{(\mathrm{3R\text{-}fit})^3O} \hat{P}_{ij}(^3O) r_{ij}^2 \exp\left(-\beta_n r_{ij}^2\right) \right]. \tag{35}$$

We fit the G3RS tensor part using this functional form and propose a new G3RS-like tensor interaction in a convenient form. The details of the fitting are explained in Appendix A. The parameter sets of all three tensor interactions are summarized in Table I. The radial part of the ^3E and ^3O components of the G3RS tensor part, the Furutani tensor, and the new three-range fit (3R fit) of the G3RS tensor part are compared in Fig. 1.

D. Parametrization of the interactions

In this paper, we compare the results of different parameter sets for the central and tensor interactions, which give major contributions to the binding energy, while the spin-orbit and Coulomb parts are fixed.

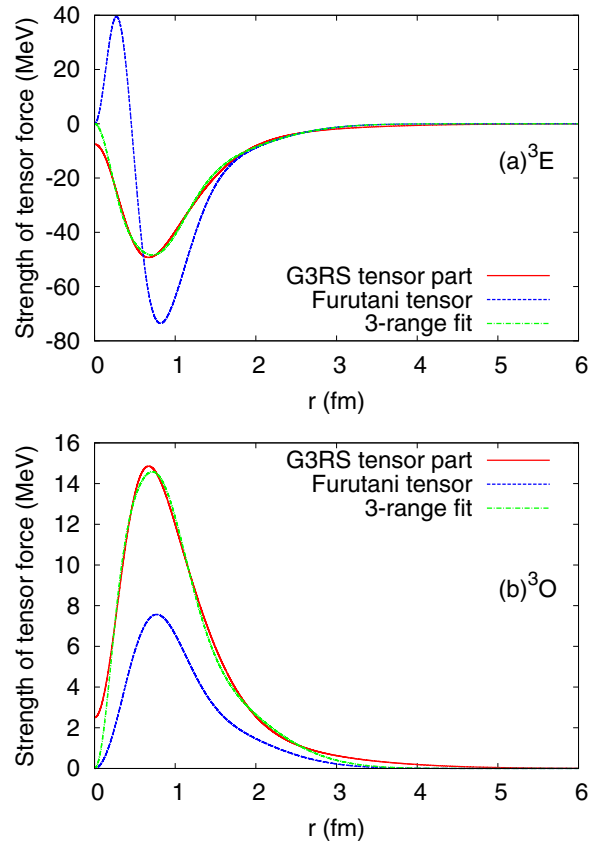

FIG. 1. The comparison of the radial part of the G3RS tensor term (solid line), Furutani tensor (dotted line), and three-range fit (dash-dotted line). (a) Triplet even part, (b) triplet odd part.

As mentioned previously, the Volkov interaction is a phenomenological central interaction, and the tensor contribution is effectively renormalized. Therefore, if we just add the tensor interaction to the Volkov interaction, the tensor effect is double counted. In this study, we weaken the Volkov interaction for the central part and add the tensor term, which reasonably reproduces energies of ^{4}He and two-nucleon systems.

We start with the Volkov no. 2 interaction with $m = 0.6$, $w = 1 - m$, $b = h = 0.15$. This parameter set is called "V2" and is often used in the conventional cluster models. This set has been known to reproduce the energy and radius of $^4\mathrm{He}_{\mathrm{gs}}$, and also the α-α scattering phase shift within the $(0s)^4$ configuration for the α cluster(s). The Bartlett and Heisenberg parameters of $b = h = 0.15$ are chosen so as to reproduce the NN scattering lengths of ^1S and ^3S without the tensor interaction as $a_s = -24$ and $a_t = 5.4$ fm, respectively (the experimental values are $a_s = -18.5 \pm 0.4$ fm [51] and $a_s = -23.749 \pm 0.008$ fm [50] for the nn and pn channels, respectively, and $a_t = 5.423 \pm 0.005$ fm [51]).

Now we combine the modified V2 interaction for the central part and the three-range fitted G3RS interaction for the tensor part. In the original V2 interaction, the large tensor contribution is effectively renormalized in the ^3E central term.

TABLE II. The parameter sets of the different combinations of the tensor and central interactions. The ^1S scattering length (a_s) and the deuteron properties (binding energy ϵ_d and D-state probability P_D) for each interaction set are shown. The column V_c is for the central interactions, and the column V_t is for the tensor interactions. The V2m interaction is the modified version of Volkov no. 2 newly introduced in the present study. The experimental data for the two-nucleon system are $a_s = -23.749 \pm 0.008$ fm for the pn channel [50] ($a_s = -18.5 \pm 0.4$ fm for the nn channel [51]) and $-\epsilon_d = 2.22$ MeV.

	V2m-3R	V2-3R	V2-F	V2
V_c	V2m	V2	V2	V2
V_t	3R fit	3R fit	Furutani	
a_s (fm)	−24	−24	−24	−24
ϵ_d (MeV)	−4.38	−11.02	−18.46	−2.65
P_D	4.9%	6.0%	8.7%	

As a result, the ^3E part of the V2 interaction with $b = h = 0.15$ is much stronger than the ^1E part, as the ratio of $^3E/^1E = 1.3/0.7$, inconsistent to the realistic interactions. To avoid double counting of the tensor contribution, we reduce the ^3E part by introducing a factor $\delta_{^3E}$ as

$$\hat{V}_c^{(\mathrm{V2m})} = (1 - (1 - \delta_{^3E})\hat{P}_{ij}(^3E))\hat{V}_c^{(\mathrm{V2})}, \tag{36}$$

where $\hat{V}_c^{(\mathrm{V2})}$ is the original V2. We adopt $\delta_{^3E} = 0.6$ (reduction of the ^3E part to 60% of the original strength) which gives the reasonable binding energy of $^4\mathrm{He}_{\mathrm{gs}}$ within the AQCM-T after including the tensor interaction. This modified central interaction is labeled as "V2m." After the reduction, the ^3E strength becomes almost the same as the ^1E one with the ratio of $^3E/^1E = 0.78/0.7$. Then we add the three-range fitted G3RS tensor interaction. We label the newly constructed interaction containing the central and tensor interactions as "V2m-3R."

We also introduce other two interactions by just adding tensor interactions to the V2 interaction without any reduction and compare the results with that obtained by the V2m-3R interaction. One is the "V2-3R" interaction, in which the three-range fitted G3RS tensor interaction is added to the V2 interaction. The other is "V2-F," where the Furutani tensor interaction is added to V2.

The parameter sets for these four interactions (V2m-3R, V2-3R,V2-F, and V2) are summarized in Table II. The ^1S scattering length and the deuteron properties (binding energy and D-state probability) obtained with these interactions are also shown. It should be commented that our newly constructed interaction, V2m-3R, gives reasonable results for the low-energy properties of both ^1E and ^3E channels, whereas the V2 interaction combined with the tensor interactions has the overbinding problem of the deuteron, because of the double counting of the tensor effect in the ^3E channel. However, the deuteron energy of V2m-3R (−4.38 MeV) is much deeper compared with the experimental value of −2.224 566 MeV. We may need further improvement of the model wave function and fine tuning of the central part.

TABLE III. Energies, radii, and probabilities of ^{4}He obtained with AQCM-T full configurations and the V2m-3R, V2-3R, and V2-F interactions together with the experimental energy and radius [52]. The result for the $(0s)^4$ state with the V2 interaction is also shown [V2:$(0s)^4$]. In V2m-G3RS, V2m is used for the central part, and the precise (20-range) fit of G3RS tensor part is used. See Appendix A for the precision of the 20-range fit.

	V2m-3R	V2-3R	V2-F	V2:$(0s)^4$	V2m-G3RS	Expt.
E (MeV)	−30.3	−52.6	−69.2	−27.9	−30.7	−28.296
T (MeV)	64.6	72.3	86.1	46.7	64.9	
V_c (MeV)	−56.7	−83.3	−85.1	−75.3	−56.7	
V_t (MeV)	−39.9	−43.2	−72.2	0.0	−40.6	
R_m (fm)	1.46	1.38	1.33	1.50	1.46	1.455
$\mathcal{P}_{0s}$	0.901	0.867	0.801	1.00	0.899	
$\mathcal{P}_{^3D}$	0.077	0.082	0.112		0.079	
$\mathcal{P}^{\perp}_{^3S}$	0.018	0.050	0.086		0.019	
$\mathcal{P}^{\perp}_{^1S}$	0.004	0.016	0.027		0.004	

IV. RESULTS OF ^{4}He

A. Properties of ^{4}He

Properties of $^4\mathrm{He}_{\mathrm{gs}}$ obtained with the AQCM-T and V2m-3R, V2-3R, and V2-F interactions are shown in Table III. The total energy (E), contributions of the kinetic term (T), central (V_c) and tensor (V_t) interactions, root-mean-square (rms) matter radii (R_m), and $0s$, ^1S, ^3S, and ^3D probabilities are listed. The result calculated with the single $(0s)^4$ configuration ($\Phi^{0s}_{^4\mathrm{He}}$) using the V2 interaction is also shown for comparison.

For V2-3R (V2-F), ^{4}He is unrealistically overbound as seen in much larger binding energy of $-E = 52.6$ MeV ($-E = 69.2$ MeV) and the smaller radius of $R_m = 1.38$ fm ($R_m = 1.33$ fm) compared with the experimental values of $-E = 28.296$ MeV and $R_m = 1.455$ fm, because of extra attraction by the strong tensor interaction (tensor effect is already renormalized in the V2 interaction).

On the contrary, the V2m-3R interaction gives the reasonable binding energy of $-E = 30.3$ MeV, because the ^3E central term is reduced to 60% of the V2 interaction. In the present paper, we use this V2m-3R as the default parameter set of the interaction, though it is possible to fine-tune the reduction factor to exactly reproduce the experimental binding energy. In practical calculations of heavier systems, possible truncations of the model space may be required to save computational costs. Therefore, this reduction factor for the ^3E central term can be regarded as an adjustable parameter, which may depend on the model space adopted.

It is quite instructive to compare the contribution of each term of the Hamiltonian obtained in two different cases: the AQCM-T with V2m-3R and the $(0s)^4$ configuration with V2; the latter is the nuclear interaction containing only the central part. The total energy is almost the same; however, the contributions of T, V_c, and V_t are much different. The contribution of the central interaction is reduced by ∼20 MeV in V2m-3R, because of the weaker ^3E central interaction compared with that in V2. The remarkable feature of V2m-3R is that a large gain of the tensor energy compensates this reduction and even overcomes the increase of the kinetic energy. It

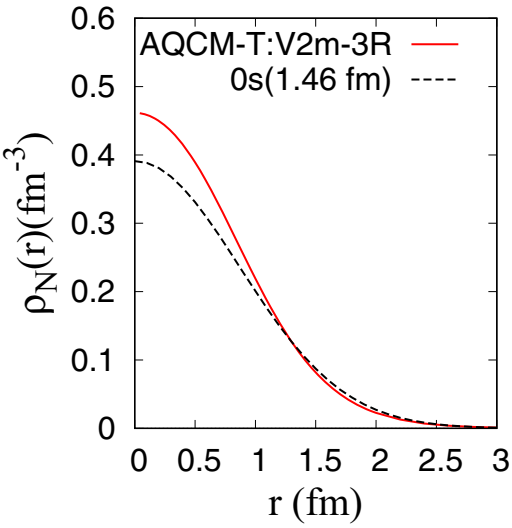

FIG. 2. Matter density distribution of ^{4}He$_{gs}$ obtained with AQCM-T and V2m-3R. The single Gaussian shape for the $(0s)^4$ configuration with $\nu = 0.264$ fm^{-2} that gives the equivalent radius 1.46 fm is also drawn.

should be stressed that this effect is attributed to the D-state mixing with the dominant S-state component. Although the D-state mixing is only 8%, the second order perturbation causes significant gain of the tensor energy through the ^3S-^3D coupling.

The AQCM-T calculation with V2m-3R gives the radius of $R_m = 1.46$ fm, which well agrees with the experimental rms point-proton radius, 1.455 fm, reduced from the observed charge radius. The matter density distribution is shown in Fig. 2 together with the single Gaussian shape [the $(0s)^4$ configuration with $\nu = 0.264$ fm^{-2} that gives the equivalent radius of $R_m = 1.46$ fm]. About 10% enhancement of the central density is obtained in the AQCM-T calculation, because of the NN correlations beyond the simple $(0s)^4$ configuration.

In Table III, we also show the result of the G3RS tensor interaction combined with the V2m interaction (labeled as "V2m-G3RS"), which are practically calculated by using the precise (20-range) fit of the G3RS tensor part. One can see that the three-range fit used in V2m-3R gives an almost equivalent contribution of each term of the Hamiltonian compared with the 20-range fit.

As explained in Sec. II, we use the fixed value of $\nu = 0.25$ fm^{-2} as the width parameter in the present article in order to compare results within the same model space. If the ν is optimized so as to minimize the total energy of ^{4}He, the value is slightly changed to $\nu = 0.24$ fm^{-2} for V2m-3R. The ν dependence of the result for ^{4}He is shown in Appendix B. In the case of the optimized value of $\nu = 0.24$ fm^{-2}, we obtain the total energy $E = -30.3$ MeV, kinetic energy $T = 63.8$ MeV, central interaction $V_c = -56.2$ MeV, tensor interaction $V_t = -39.5$ MeV, radius $R_m = 1.47$ fm, and D-state probability $\mathcal{P}_{^3D} = 0.078$. Nevertheless the differences from the results of the fixing ν to $\nu = 0.25$ fm^{-2} in Table III are only 1% at most in the case of V2m-3R.

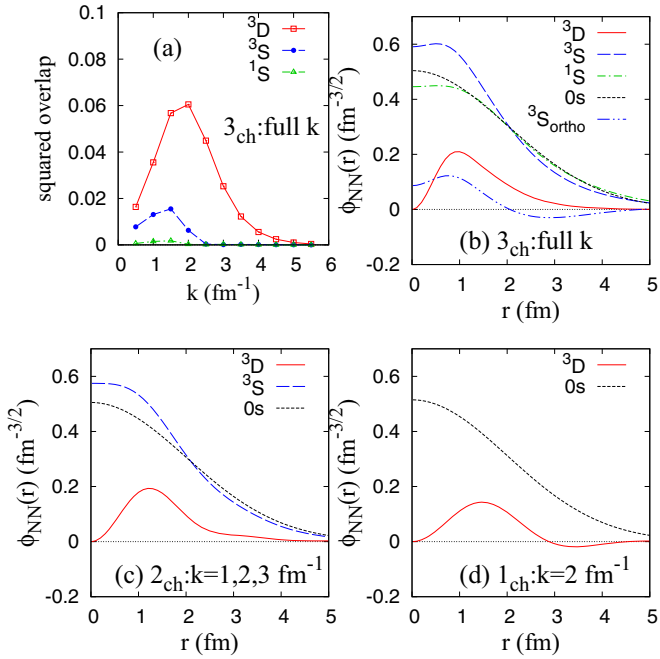

FIG. 3. The squared overlaps $\mathcal{O}_\beta(k)$ and pair wave functions $\phi_{NN}(r)$ in ^{4}He$_{gs}$ calculated with AQCM-T and the V2m-3R interaction. (a) Squared overlaps obtained by the full calculation (three-channel calculation with full k configurations, $k = \{0.5, 1.0, \ldots, 5.5\}$ fm^{-1}); (b) pair wave functions in the ^3D, ^3S, and ^1S, and $0s$ components obtained by the full calculation; (c) those obtained by the two-channel calculation with $k = \{1, 2, 3\}$ fm^{-1}; (d) those obtained by the single-channel calculation with $k = 2$ fm^{-1}. In (b), the ^3S pair wave functions in the $(0s)^4$ configuration and that ($^3S_{\rm ortho}$) in the orthogonal configuration $(1 - |0s\rangle\langle 0s|)|\Psi_{^4\mathrm{He,gs}}\rangle$ are also shown.

B. NN correlations in ^{4}He

1. Contributions of correlated NN pairs

Next, we discuss the NN correlations in ^{4}He, which are incorporated in the present AQCM-T calculation by introducing the correlated NN pairs. Figure 3(a) shows the squared overlap ($\mathcal{O}_\beta$) of $\Psi_{^4\mathrm{He,gs}}$ with each basis state of the AQCM-T specified by k and β shown in Eq. (19). The overlap with the ^3D channel is calculated as

$$\mathcal{O}_{^3D}(k) = \left|\left\langle \Phi^{\mathrm{AQCM\text{-}T}}_{^4\mathrm{He},0^+}(k, {}^3D)\middle|\Psi_{^4\mathrm{He,gs}}\right\rangle\right|^2. \quad (37)$$

The overlaps with the $^{1,3}S$ channels are defined for the space orthogonal to $|0s\rangle$ as

$$\mathcal{O}_{^{1,3}S}(k) = \left|\left\langle \Phi^{\mathrm{AQCM\text{-}T}}_{^4\mathrm{He},0^+}(k, {}^{1,3}S)\Lambda^{\perp}_{0s}\middle|\Psi_{^4\mathrm{He,gs}}\right\rangle\right|^2. \quad (38)$$

This is to measure the correlated $^{1,3}S$ components beyond the simple $(0s)^2$ pair. The ground state ($\Psi_{^4\mathrm{He,gs}}$) has the largest overlap with the correlated ^3D pair at $k \sim 1.5$–2.0 fm^{-1}, indicating that the intermediate momentum dominantly contributes to the tensor correlation. The present result is qualitatively consistent with the result of Ref. [44], in which the interactions are almost equivalent to V2-F of the present paper. But quantitatively speaking, the result with V2m-3R is more or less different from that with V2-F; in the latter

TABLE IV. Energies, radii, and probabilities of ^{4}He obtained with the truncated configurations using the V2m-3R interaction. The results obtained by three-, two-, single-channel calculations with full k configurations ($k = \{0.5, 1.0, \ldots, 5.5\}$ fm^{-1}), the two-channel calculation with $k = \{1, 2, 3\}$ fm^{-1}, and single-channel calculation with $k = 2$ fm^{-1} are shown together with the result for the $(0s)^4$ state.

β	$3_{\rm ch}$	$2_{\rm ch}$	$1_{\rm ch}$	$2_{\rm ch}$	$1_{\rm ch}$	$(0s)^4$
k	$\{^1S, ^3S, ^3D\}$	$\{^3S, ^3D\}$	$\{^3D\}$	$\{^3S, ^3D\}$	$\{^3D\}$	
	full	full	full	$\{1, 2, 3\}$	$\{2\}$	
E (MeV)	-30.3	-30.0	-28.2	-28.2	-23.1	-8.3
T (MeV)	64.6	65.7	58.9	64.8	56.4	46.7
$V_{\rm c}$ (MeV)	-56.7	-57.1	-53.7	-57.4	-54.0	-55.8
$V_{\rm t}$ (MeV)	-39.9	-40.2	-35.0	-37.3	-26.9	0.0
R_m (fm)	1.46	1.44	1.49	1.43	1.50	1.50
$\mathcal{P}_{0s}$	0.901	0.903	0.927	0.905	0.940	1.00
$\mathcal{P}_{^3D}$	0.077	0.078	0.073	0.080	0.060	
$\mathcal{P}^{\perp}_{^3S}$	0.018	0.019		0.016		
$\mathcal{P}^{\perp}_{^1S}$	0.004					

case the dominant contribution shifts to a slightly higher region of k, around $k \sim 2$ fm^{-1}. This interaction gives unrealistically overbound ^{4}He, because the tensor interaction is already renormalized in the central part of V2-F. It is worth mentioning that $\Psi_{^4{\rm He,gs}}$ has finite overlap with the correlated ^3S pair, which gives a non-negligible contribution to the tensor correlation, as discussed later.

In order to clarify the contribution and role of each channel and basis state, we perform the AQCM-T calculations within truncated model spaces. At first, we truncate the channels, $\beta = \{^1S, ^3S, ^3D\}$, which is the truncation of the spin-isospin space; we omit the $\{^1S\}$ and $\{^1S, ^3S\}$ channel(s) and perform two- and single-channel calculations using only $\beta = \{^3S, ^3D\}$ and $\{^3D\}$ channel(s), respectively, whereas we employ all the basis states for the k values in Eq. (19). In Table IV, the results of two- and single-channel calculations with the V2m-3R interaction are listed and compared with the those of the three-channel ($\beta = \{^1S, ^3S, ^3D\}$) calculation. The two-channel calculation gives quite a similar result to the full (three-channel) one, indicating there is almost no effect of the ^1S correlation. However, if we compare the two-channel and single-channel calculations, it can be seen that the ^3S truncation gives significant effects on the T, $V_{\rm c}$, and $V_{\rm t}$ energies, even if it gives a minor effect on the total energy E. For instance, the $V_{\rm t}$ contribution is suppressed by about 5 MeV when the correlated ^3S component is missing since it directly couples with the NN pair in the ^3D state with $T = 0$. Although the ^3D component plays a primary role in the tensor correlation, the coupling of the two channels, ^3S and ^3D, is necessary to quantitatively describe the features of the tensor correlation. The single-channel calculation only describes basic features of ^{4}He, such as tensor contribution in energy or D-state probability, qualitatively.

For comparison, we also show the results of three-, two-, and single-channel calculations obtained with the V2-F interaction in Table V. Unlike the V2m-3R case, the inclusion of the correlated ^3S component significantly contributes to all energy terms (E, T, $V_{\rm c}$, and $V_{\rm t}$) as well as the D-state probability. However, it may be an artifact because of the unrealistic overbinding of ^{4}He due to the double counting of the tensor contribution in the central and tensor terms.

TABLE V. Energies, radii, and probabilities of ^{4}He obtained with truncated configurations using the V2-F interaction. The results of three-, two-, single-channel calculations with full k configurations are listed.

β	$3_{\rm ch}$	$2_{\rm ch}$	$1_{\rm ch}$
k	$\{^1S, ^3S, ^3D\}$	$\{^3S, ^3D\}$	$\{^3D\}$
	full	full	full
E (MeV)	-69.2	-68.9	-60.3
T (MeV)	86.1	85.5	65.1
$V_{\rm c}$ (MeV)	-85.1	-84.4	-73.1
$V_{\rm t}$ (MeV)	-72.2	-72.1	-54.2
R_m (fm)	1.33	1.33	1.49
$\mathcal{P}_{0s}$	0.801	0.803	0.902
$\mathcal{P}_{^3D}$	0.112	0.112	0.098
$\mathcal{P}^{\perp}_{^3S}$	0.086	0.085	
$\mathcal{P}^{\perp}_{^1S}$	0.027		

Next, we truncate the k values in Eq. (19); we perform the two-channel ($\beta = \{^3S, ^3D\}$) calculations with reduced number of the basis states with different k values. Here we employ only three values of $k = \{1, 2, 3\}$ fm^{-1} for the ^3S and ^3D channels, which represent the important features of the ground state of ^{4}He and cover most of the functional space, as one can see in Fig. 3(a), the overlap with the full calculation. As expected, the two-channel calculation only with $k = \{1, 2, 3\}$ fm^{-1} efficiently describes the properties of ^{4}He in the level almost comparable to the full calculation. On the other hand, when we further reduce the model space and perform the single-channel calculation with a single $k = 2$ fm^{-1} configuration, we obtain the binding energy of $-E = 23.1$ MeV. This energy is much lower compared with $-E = 8.3$ MeV of the pure $(0s)^4$ case owing to the mixing of the single correlated configuration; however, compared with the full calculation, the $V_{\rm t}$ contribution is significantly reduced, indicating that superposition of different k configurations in the ^3S and ^3D channels is important to quantitatively describe the tensor correlation.

2. Pair wave functions

Using the partial wave expansion of $\varphi^+_k(\boldsymbol{r})$ shown in Eq. (10), we reconstruct the intrinsic wave function of the correlated NN pair, which we call the pair wave function $\phi_{NN}(r)$. The pair wave functions $\phi_{NN}(r)$ defined here are those for the NN pair with correlations in the ^1S, ^3S, and ^3D components of $\Psi_{^4{\rm He,gs}}$ as

$$^1S : \phi_{NN}(r)\varphi^{(0)}_0(r') \otimes Y_{00}Y_{00} \otimes \chi^{\sigma}_0\chi^{\sigma}_0 \otimes \left[\chi^{\tau}_1\chi^{\tau}_1\right]_{T=0},$$

$$^3S : \phi_{NN}(r)\varphi^{(0)}_0(r') \otimes Y_{00}Y_{00} \otimes \left[\chi^{\sigma}_1\chi^{\sigma}_1\right]_{S=0} \otimes \chi^{\tau}_0\chi^{\tau}_0,$$

and

$$^3D : \phi_{NN}(r)\varphi^{(0)}_0(r') \otimes \left[Y_{20}Y_{00} \otimes \left[\chi^{\sigma}_1\chi^{\sigma}_1\right]_{S=2}\right]_{J=0} \otimes \chi^{\tau}_0\chi^{\tau}_0,$$

respectively. They are given by the linear combination of $\varphi^{(0)}_k(r)$ or $\varphi^{(2)}_k(r)$, respectively, and their Fourier

transformation is related to the overlap $\mathcal{O}(k)$ of the corresponding channel. Figure 3(b) shows the pair wave functions $\phi_{NN}(r)$ in the ground state ($\Psi_{^4\mathrm{He,gs}}$) obtained with the full AQCM-T basis states and the V2m-3R interaction. The ^3S pair wave function in the $(0s)^4$ configuration projected from the ground state ($|0s\rangle\langle 0s|\Psi_{^4\mathrm{He,gs}}\rangle$) and that in the orthogonal correlated component $[(1-|0s\rangle\langle 0s|)|\Psi_{^4\mathrm{He,gs}}\rangle]$ are also shown. The pair wave function in the ^3D component has a peak around the $r\sim 1$ fm region and shows a tail behavior in the $2\lesssim r\lesssim 3$ fm region. The amplitude at the peak in the short distances is represented by high k components, whereas the long-range tail is expressed by low k components. It is also interesting to see that the ^3S pair wave function shows a significant enhancement around $r\sim 1$ fm, consistent with the peak position of the ^3D pair wave function. The enhancement of the ^3S pair wave function in this region is caused by the ^3S-^3D coupling attributed to the tensor interaction, which effectively provides an extra attraction for the ^3S channel. This ^3S-^3D coupling gives the answer why mixing of the correlated ^3S component has a significant effect on the tensor correlation in ^{4}He, discussed previously.

For a more quantitative discussion on the spatial extent of the ^3D pair, we calculate the rms distance of the pair wave function defined as

$$r_{\mathrm{pair}}\equiv\sqrt{\int drr^4|\phi_{NN}(r)|^2\Big/\int drr^2|\phi_{NN}(r)|^2}. \qquad (39)$$

We obtain $r_{\mathrm{pair}}=1.70$ fm for the ^3D pair, which is smaller than $r_{\mathrm{pair}}=2.24$ fm for the ^3S pair [for the ^3S pair in the pure $(0s)^4$ state, $r_{\mathrm{pair}}=\sqrt{3/(2\nu)}=2.45$ fm].

Since the enhancement of the ^3D and ^3S pair wave functions are seen in the $r\lesssim 2$ region, we can say that this region is of special importance for the $T=0$ pair because of the tensor correlation. This region of $r\lesssim 2$ for the NN pair roughly corresponds to the internal area of $r_i\lesssim 1$ fm for the total ^{4}He system.

Let us turn to the pair wave functions $[\phi_{NN}(r)]$ obtained by using truncated model space. Figure 3(c) shows $\phi_{NN}(r)$ for the two-channel ($\beta=\{^3S,^3D\}$) calculation with $k=\{1,2,3\}$ fm^{-1}, and Fig. 3(d) shows that for the single-channel ($\beta=^3D$) calculation with $k=2$ fm^{-1}. In the two-channel calculation with $k=\{1,2,3\}$ fm^{-1}, $\phi_{NN}(r)$ shows similar behaviors to that of the full calculation, that is, the appearance of short-range peak and long-range tail for ^3D and short-range enhancement for ^3S. On the other hand, in the single-channel calculation with $k=2$ fm^{-1}, somewhat different features of the pair wave function are seen. The ^3D pair wave function shows a short-range peak, but it is milder and slightly shifted toward the outer region, $r\sim 1.5$ fm, than that of the full calculation. Moreover, in the long distance region, the pair wave function has a negative amplitude instead of the gradually decreasing tail obtained in the full calculation. The reason is that a single k configuration for the ^3D channel is not enough and it gives an oscillating function of $\varphi_k^{(2)}(r)$ with the $e^{-(\nu/2)r^2}j_2(kr)$ dependence.

The present analysis indicates that the superposition of different k configurations in a wide momentum space is essential for detailed description of the tensor correlation, even though the contribution of $k\sim 2$ fm^{-1} is dominant. In particular, higher k components in the ^3S and ^3D channels, typically $k\gtrsim 3$ fm^{-1}, are necessary for precisely describing the tensor correlation at the shorter range around $r\sim 1$ fm of the $T=0$ pair.

V. RESULTS OF ^{8}Be

In this section, we investigate the tensor correlations in ^{8}Be with a two α configuration, where the V2m-3R interaction is adopted. Here, the AQCM-T is applied to one of the α clusters, and we adopt only two channels, $\beta=\{^3S,^3D\}$ with $k=\{1,2,3\}$ fm^{-1}.

In Fig. 4, we show the energies of ^{8}Be as a function of d_α, which is the parameter for the relative distance between two α clusters, (a) total energy, (b) probabilities of the $0s$ and ^3D configurations, (c) contribution of each component of the Hamiltonian. In (c) and (d), the relative energies are measured from values at $d_\alpha=7$ fm. Also we list in Table VI the values for the contribution of each term of the Hamiltonian and the probabilities of the $0s$ and ^3D configuration as functions of d_α. The results calculated with BB cluster model with V2 interaction are shown in Figs. 4(a) and 4(d) and Table VI for comparison. In Fig. 4(a) and Table VI, we also show the ideal values of the asymptotic energies corresponding to the ones at $d_\alpha\to\infty$, evaluated as twice the ^{4}He energy calculated with the consistent model space, i.e., the two-channel calculation

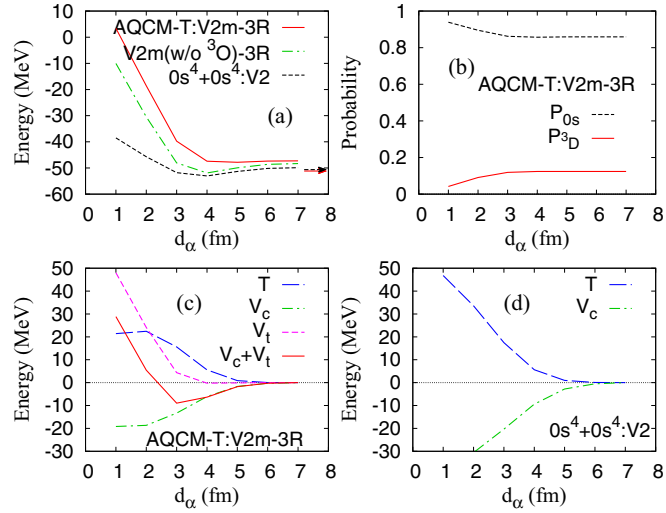

FIG. 4. Energy and the probabilities of $0s$ and D states in ^{8}Be calculated with AQCM-T and the V2m-3R interaction, as a function of the relative distances d_α between the two α clusters, (a) total energy, (b) $0s$ and ^3D probabilities, and (c) energy of each component of the Hamiltonian. The total energy calculated using the V2m central interaction without the odd part combined with the three-range fit tensor interaction is also shown in (a). The results calculated with the BB cluster model and V2 are shown in (a) and (d). In panel (a), the asymptotic energy for AQCM-T and BB are shown by arrows. The energy calculated with AQCM-T using the V2m central interaction without the odd part combined with the three-range fit tensor interaction is also shown in (a). In (c) and (d), the relative energies measured from $d_\alpha=7$ fm are plotted.

TABLE VI. Energy for each component of the Hamiltonian and the probabilities of $0s$ and D-states in ^{8}Be calculated with AQCM-T and the V2m-3R interaction, as a function of the relative distances d_α between the two α clusters (upper column). The asymptotic and threshold energies are given as twice the ^{4}He energy calculated with a consistent model space. For the asymptotic values, the constant shift of $T_r = \hbar\omega/4 = 5.2$ MeV is added for the kinetic and total energies, corresponding to the localization of clusters with fixed relative distance. The asymptotic value of the $0s$ probability given by the square of $\mathcal{P}_{0s}$ for ^{4}He is also shown. The results obtained by the BB 2α cluster model with the V2 interaction are also shown (lower column).

AQCM-T:V2m-3R						
d_α	$\langle E\rangle_{2\alpha}$	$\langle T\rangle_{2\alpha}$	$\langle V_c\rangle_{2\alpha}$	$\langle V_t\rangle_{2\alpha}$	$\mathcal{P}_{0s}$	$\mathcal{P}_{^3D}$
1	3.4	148.1	−132.8	−16.1	0.94	0.04
2	−18.6	149.1	−132.3	−40.0	0.90	0.09
3	−39.7	142.3	−127.0	−59.8	0.86	0.12
4	−47.4	132.3	−119.7	−64.4	0.86	0.12
5	−47.8	127.6	−115.3	−64.2	0.86	0.12
6	−47.4	126.7	−113.9	−64.1	0.86	0.12
7	−47.3	126.7	−113.7	−64.1	0.86	0.12
	$2\langle E\rangle_\alpha + T_r$	$2\langle T\rangle_\alpha + T_r$	$2\langle V_c\rangle_\alpha$	$2\langle V_t\rangle_\alpha$	$\{\mathcal{P}_{0s}\}^2_\alpha$	
Asymptotic	−51.2	134.9	−114.9	−74.5	0.82	
2α threshold	−56.4					

BB:V2			
d_α (fm)	$\langle E\rangle_{2\alpha}$	$\langle T\rangle_{2\alpha}$	$\langle V_c\rangle_{2\alpha}$
1	−38.5	145.3	−187.6
2	−45.7	132.1	−181.4
3	−51.8	116.0	−171.1
4	−53.0	104.1	−160.2
5	−51.3	99.5	−153.5
6	−50.2	98.6	−151.3
7	−49.9	98.5	−150.8
	$2\langle E\rangle_\alpha + T_r$	$2\langle T\rangle_\alpha + T_r$	$2\langle V_c\rangle_\alpha$
Asymptotic	−50.6	98.5	−150.7
2α threshold	−55.8		

with $k = \{1, 2, 3\}$ fm^{-1}. Note that here the constant shift of $T_r = \hbar\omega/4$ ($=\hbar^2\nu/2m$, m is the mean value of proton and neutron masses) is added for the kinetic and total energies, which corresponds to the increase of the kinetic energy due to the localization of the intercluster motion around d_α.

In Table VI, we can confirm that the two α system largely gains the tensor contribution in the $d_\alpha \geqslant 6$ fm region with the significant mixing of ^3D and dominant $0s$ components. The energy of each component of the Hamiltonian in this region is almost comparable to the asymptotic values indicating that the two α system is approaching a weak coupling $^4\mathrm{He}_{\mathrm{gs}} + {}^4\mathrm{He}_{\mathrm{gs}}$ state. However, small deviations from the asymptotic values still remain, because in the present model with the $\alpha_k + \alpha_0$ cluster wave functions, higher order correlations of $\alpha_k + \alpha_k$ configurations, where both clusters contain the correlated $T = 0$ NN pair, are omitted.

As seen in Table VI and Fig. 4(a), in the region of $d_\alpha \leqslant 3$ fm, the system gets more excited as the α-α distance (d_α) becomes smaller. In particular, in the $d_\alpha \leqslant 2$ fm region, the total energy rapidly increases, because the tensor correlation is remarkably suppressed as can be seen in the reductions of V_t and ^3D in Table VI and Fig. 4(b). Namely, although the V_t contribution stays almost constant in the $d_\alpha \geqslant 3$ fm region, it rapidly decreases in the shorter region, the $d_\alpha \geqslant 2$ fm, as the α clusters come close to each other. Also, the ^3D probability is almost unchanged in the $d_\alpha \geqslant 3$ fm region, but it rapidly decreases in the $d_\alpha \leqslant 2$ fm region. This means that the suppression of the tensor correlation strongly contributes to the repulsion between two α clusters at short distances. On the other hand, the total energy starts increasing already around $d_\alpha \sim 3$ fm, and its origin is the increase of the kinetic energy rather than the tensor suppression. In other words, in the α-α energy curve, the tensor suppression contributes to the repulsion at a relatively short range between two α clusters, whereas the increase of the kinetic energy contributes in the longer range. These two repulsive effects enhance the characteristic development of the two α cluster structure in ^{8}Be.

Both of these repulsive effects between two α clusters can be understood as the realization of the Pauli blocking effect, but they come from different origins. Indeed, the longer-range one can be seen even in the BB calculation, because it comes from the increase of the kinetic energy due to the Pauli blocking between $0s$-orbit nucleons in the α cluster and that in the other α cluster. However, the shorter-range one comes from the tensor suppression, which is the blocking of $(0s)^{-2}(0p)^2$ excitations induced by the tensor interaction in the correlated α cluster by the other α cluster. As discussed in the analysis for ^{4}He, the spatial extension of the tensor correlated NN pair is relatively smaller than the typical range of the uncorrelated NN pair in the $(0s)^4$ state. As a result, the tensor suppression occurs only when two α clusters are close enough to block the particle hole excitation of the correlated pair with a compact distribution. This scenario of the tensor suppression and the consequent appearance of the two α cluster structure is consistent with the ones already proposed and discussed quite a long time ago [12,14]. We also discussed a similar effect for the tetrahedron configuration of four α clusters in ^{16}O that the finite distance between α clusters is favored due to the tensor suppression [43].

As seen in Fig. 4(a), the BB calculation with V2 (dotted line) gives a shallow energy pocket around $d_\alpha = 3 \sim 4$ fm. However, in the present calculation with the V2m-3R interaction, this energy pocket disappears because of the weaker central interaction. If we remove the odd part of the central interaction, we obtain an energy pocket with almost the same depth as the V2 interaction [see the dash-dotted line of Fig. 4(a)]. Note that this change of the odd part of the central interaction keeping the even part unchanged gives almost no effect to the ^{4}He results. Fine tuning of the central interactions, in particular the odd part, is a remaining problem for the study of heavier systems in the near future.

VI. SUMMARY

In this paper, we directly treated the tensor interaction and examined the effect in ^{4}He and ^{8}Be. We extend the framework of *i*SMT and the newly proposed AQCM-T, the tensor version

of the AQCM. Although the AQCM-T is a phenomenological model, we can treat the ^3S-^3D coupling in the deuteronlike $T = 0$ NN pair induced by the tensor interaction in a very simplified way, which allows us to proceed to heavier nuclei. The model is also regarded as a specific version of the HM-AMD. In the previous analyses based on the iSMT and HM-AMD, the tensor interaction was just added to the effective Hamiltonian, and the tensor effect was double counted. In this study, we examined the case of an effective interaction, V2m, where the triplet-even part of the central interaction (V2) was reduced to 60% of the original strength so as to reproduce the correct binding energy of ^{4}He within the AQCM-T model space. For the tensor term, G3RS interaction was adopted, which was refitted using three Gaussians with a factor of r^2. This combination of the central and tensor interactions is called V2m-3R.

For ^{4}He, the two results of the AQCM-T with V2m-3R and $(0s)^4$ configuration with V2 give almost the same total energy, however, the contributions of each component of the Hamiltonian are much different. The contribution of the central interaction is reduced by ∼20 MeV in V2m-3R, because of the weaker triplet-even channel compared with that in V2, whereas the large gain of the tensor energy compensates this reduction and even overcomes the increase of the kinetic energy. This effect is attributed to the D-state mixing with the S state, which is still a dominant component; the ^3D probability ($\mathcal{P}_{^3D}$) is only 8%. The AQCM-T calculation with V2m-3R gives the rms matter radius of 1.46 fm, which well agrees with the value reduced from the experimental charge radius, 1.455 fm.

The present AQCM-T was also applied to ^{8}Be within the two α model space, where one of the α clusters was transformed from the $(0s)^4$ configuration using the AQCM-T. The tensor effect was investigated as a function of relative distance between α clusters, d_α, and found to give a significant contribution to the short-range repulsion between two α clusters. In the large d_α region, the contribution of each term of the Hamiltonian is almost comparable to the asymptotic values deduced from twice of the values for ^{4}He, indicating that the two α system is approaching a weak coupling, $^4\mathrm{He}_{\mathrm{gs}} + {}^4\mathrm{He}_{\mathrm{gs}}$, state. It also indicates that, although the present AQCM-T model for ^{8}Be explicitly treats the tensor correlation only in one of the α clusters, this is a good approximation at least for the two α system owing to the Bosonic nature of the α clusters.

The tensor interaction is really the key ingredient of the cluster structure. It contributes to the strong binding of the subsystems, ^{4}He, called the α cluster, and it is also related to the weak interaction between the subsystems. Furthermore, the tensor suppression in each α cluster contributes to the strong repulsion at short relative distances. This scenario of the tensor suppression and the consequent appearance of the two α cluster structure was proposed quite a long time ago, and here we have discussed it in a more direct way. It is worthwhile to investigate such an important effect of the tensor interaction in heavier nuclei, which may be possible because of the simple AQCM-T treatment proposed here. Extension of the AQCM-T for nuclear matter is also an important issue, which may be associated with the saturation property of nuclear matter.

ACKNOWLEDGMENTS

The computational calculations of this work were performed by using the supercomputer at Yukawa Institute for Theoretical Physics, Kyoto University. This work was supported by JSPS KAKENHI Grants No. 26400270 (Y.K-E.), No. 17K05440 (N.I.), No. 18J13400 (H.M.), and No. 18K03617 (Y.K-E.).

APPENDIX A: GAUSSIAN FIT FOR TENSOR FORCE

1. Determination of parameters for tensor interaction

We aim to propose a G3RS-like tensor interaction in a convenient form, which can be easily used in practical calculations; we fit the G3RS tensor force with the multirange Gaussian functional form with a factor of r^2 as follows.

The radial part of the G3RS tensor term for the ^3E or ^3O channel is

$$V_{\mathrm{t}}^{(\mathrm{G3RS})\{^3E,^3O\}}(r) = \sum_{n=1}^{3} V_{\mathrm{t},n}^{(\mathrm{G3RS})\{^3E,^3O\}} \exp\left(-\frac{r^2}{\eta_{\mathrm{t},n}^2}\right), \quad \text{(A1)}$$

and that of the $n_{\max}$-range fit introduced in this work is

$$V_{\mathrm{t}}^{(\mathrm{fit})\{^3E,^3O\}}(r) = \sum_{n=1}^{n_{\max}} V_{\mathrm{t},n}^{(\mathrm{fit})\{^3E,^3O\}} r^2 \exp(-\beta_n r^2). \quad \text{(A2)}$$

Our aim here is to fit $f(r) = V_{\mathrm{t}}^{(\mathrm{G3RS})\{^3E,^3O\}}(r)$ with $g(r) = V_{\mathrm{t}}^{(\mathrm{fit})\{^3E,^3O\}}(r)$. For this aim, we define the function F, which

TABLE VII. The parameters $\{b_n\}$ and $\{V_{\mathrm{t},n}^{(\mathrm{fit})}\}$ of the 20-range fit tensor interaction for the ^3E and ^3O channels.

n	b_n (fm)	$V_{\mathrm{t},n}^{(\mathrm{fit})}$ (MeV fm^{-2})	
		^3E	^3O
1	0.1000	−1403.1	467.67
2	0.1322	387.27	−129.09
3	0.1747	−443.05	147.72
4	0.2308	50.189	−16.847
5	0.3051	−90.076	30.307
6	0.4032	−35.449	10.705
7	0.5329	−160.83	48.483
8	0.7043	−76.453	22.860
9	0.9308	−53.823	16.165
10	1.2302	−12.189	3.6997
11	1.6258	−0.73858	0.28279
12	2.1487	−1.0741	0.34869
13	2.8398	1.2481×10^{-2}	-1.2718×10^{-3}
14	3.7531	-1.3513×10^{-2}	3.5475×10^{-3}
15	4.9602	5.0273×10^{-3}	-1.3535×10^{-3}
16	6.5555	-1.7096×10^{-3}	4.6338×10^{-4}
17	8.6638	5.3737×10^{-4}	-1.4603×10^{-4}
18	11.4503	-1.4765×10^{-4}	4.0172×10^{-5}
19	15.1329	3.1296×10^{-5}	-8.5195×10^{-6}
20	20.0000	-3.7491×10^{-6}	1.0209×10^{-6}

TABLE VIII. The values of the $\mathcal{F}^{^3E}_{S\text{-}D}$ and $\mathcal{F}^{^3O}_{P\text{-}P}$ calculated with the G3RS, Furutani, three-range fit, and 20-range fit tensor interactions.

$V_{\rm t}^{(\rm fit)\{^3E,^3O\}}(r)$	$\mathcal{F}^{^3E}_{S\text{-}D}$ (MeV)	$\mathcal{F}^{^3O}_{P\text{-}P}$ (MeV)
G3RS	−35.056	6.8319
Furutani	−44.980	3.6135
Three-range	−34.805	6.6619
20-range	−35.058	6.8323

is the square of the difference between these two integrated in the $a \leqslant r \leqslant b$ region as

$$F\left(\left\{V_{{\rm t},n}^{(\rm fit)}\right\}\right) = \int_a^b [f(r) - g(r)]^2 dr. \tag{A3}$$

We optimize the strength parameters $\{V_{{\rm t},n}^{(\rm fit)}\}$ by minimizing F, while the range parameters $\{\beta_n\}$ and the integration interval (a and b) are fixed. We construct the three-range fit ($n_{\max} = 3$) tensor interaction for the use of economical calculations. For the range parameters $\{\beta_n\}$ $(n = 1, 2, 3)$ of the three-range fit, we employ the values of the Furutani interaction, whose functional form is identical to $g(r)$. The range parameters $\{\beta_n\}$ $(n = 1, 2, 3)$ are well scattered, so it is appropriate to take $a = 1/\sqrt{\beta_3}$ and $b = 1/\sqrt{\beta_1}$ in Eq. (A3).

As shown in Fig. 1, the r dependence of the three-range fit agrees well with that of the G3RS tensor part, but the fitting precision is not perfect. We also prepare the 20-range fit ($n_{\max} = 20$) version, which fits almost perfectly. In order to reproduce the G3RS tensor part in a wide range, we choose the range parameters $b_n = b_1 \times (b_{20}/b_1)^{(n-1)/19}$ with $b_1 = 0.1$ fm and $b_{20} = 20.0$ fm, where $\beta_n = 1/b_n^2$. The parameters $\{b_n\}$ and $\{V_{{\rm t},n}^{(\rm fit)}\}$ of the 20-range fit are shown in Table VII.

2. Precision of the fitting

To evaluate the precision of the fitting for the radial part of the tensor interactions $V_{\rm t}^{(\rm fit)\{^3E,^3O\}}(r)$, we calculate the matrix element

$$\mathcal{F} = \langle \psi_f | \hat{V}_{\rm t} | \psi_i \rangle, \tag{A4}$$

where $\psi_{i,f}$ is the normalized relative wave function for the NN pair. For the ^3E channel, the dominant contribution to the energy of ^{4}He comes from the S-D coupling in the ^3E pair through the nondiagonal matrix element of the tensor interaction. In particular, the coupling of the ^3D component with $k = 2$ fm^{-1} with the ^3S component is important as shown in the present AQCM-T result of ^{4}He. The corresponding matrix element is calculated as

$$\begin{aligned}\mathcal{F}^{^3E}_{S\text{-}D} &= \sqrt{8}\int_0^\infty \varphi_k^{(2)}(r) V_{\rm t}^{^3E}(r) \varphi_{k=0}^{(0)}(r) r^2 dr \\ &\propto \sqrt{8}\int_0^\infty V_{\rm t}^{^3E}(r) e^{-(\nu/2)r^2}\left[e^{-(\nu/2)r^2} j_2(kr)\right] r^2 dr,\end{aligned} \tag{A5}$$

where $\varphi_k^{(l)}(r)$ is the normalized radial wave function in Eq. (10) and proportional to $e^{-(\nu/2)r^2} j_l(kr)$. For the ^3O channel, we evaluate here the diagonal matrix element for the ^3P pair contained in the D state of ^{4}He using the ADCM-T wave function with $k = 2$ fm^{-1} as

$$\begin{aligned}\mathcal{F}^{^3O}_{P\text{-}P} &= 2\int_0^\infty \varphi_k^{(1)}(r) V_{\rm t}^{^3O}(r) \varphi_k^{(1)}(r) r^2 dr \\ &\propto 2\int_0^\infty V_{\rm t}^{^3O}(r)\left[e^{-(\nu/2)r^2} j_1\left(\frac{k}{2}r\right)\right]^2 r^2 dr.\end{aligned} \tag{A6}$$

The calculated values of $\mathcal{F}^{^3E}_{S\text{-}D}$ and $\mathcal{F}^{^3O}_{P\text{-}P}$ for the G3RS, Furutani, three-range fit, and 20-range fit tensor interactions are shown in Table VIII. The values for the three-range fit well agree with those for G3RS within the accuracy of a few %. For the 20-range fit, the agreement is almost perfect meaning that it can be regarded as an equivalent potential to the G3RS tensor interaction.

TABLE IX. ν dependence of energies, radii, and D-state probability of ^{4}He obtained with AQCM-T full configurations for V2m-3R.

ν (fm^{-2})	0.23	0.24	0.25
E (MeV)	−30.32	−30.33	−30.30
T (MeV)	62.87	63.76	64.61
$V_{\rm c}$ (MeV)	−55.62	−56.17	−56.70
$V_{\rm t}$ (MeV)	−39.06	−39.49	−39.86
R_m (fm)	1.49	1.47	1.46
$\mathcal{P}_{^3D}$	0.078	0.078	0.077

APPENDIX B: ν DEPENDENCE OF ^{4}He

The dependence of the ^{4}He results on the size parameters of the Gaussian-type wave function, ν, obtained with the AQCM-T full configurations and the V2m-3R interaction, is shown in Table IX. The energy contribution of each Hamiltonian term, radius, and D-state probability calculated with $\nu = 0.23$, 0.24, and 0.25 fm^{-2} are shown. The minimum energy of ^{4}He is obtained with the optimized size parameter, $\nu = 0.24$ fm^{-2}. Comparing the results for the optimized ν value (0.24 fm^{-2}) with those for $\nu = 0.25$ fm^{-2} adopted in the present article, the differences in the energy, radius, and probability are found to be 1% at most.

[1] D. M. Brink, in *Proceedings of the International School of Physics "Enrico Fermi" Course XXXVI*, edited by C. Bloch (Academic, New York, 1966), p. 247.
[2] Y. Fujiwara, H. Horiuchi, K. Ikeda, M. Kamimura, K. Katō, Y. Suzuki, and E. Uegaki, Prog. Theor. Phys. Suppl. **68**, 29 (1980).
[3] F. Hoyle, Astrophys. J. Suppl. Ser. **1**, 12 (1954).
[4] E. Uegaki, S. Okabe, Y. Abe, and H. Tanaka, Prog. Theor. Phys. **57**, 1262 (1977).
[5] A. Tohsaki, H. Horiuchi, P. Schuck, and G. Röpke, Phys. Rev. Lett. **87**, 192501 (2001).
[6] P. Maris, J. P. Vary, and A. M. Shirokov, Phys. Rev. C **79**, 014308 (2009).

[7] A. C. Dreyfuss, K. D. Launey, T. Dytrych, J. P. Draayer, and C. Bahri, Phys. Lett. B **727**, 511 (2013).
[8] T. Yoshida, N. Shimizu, T. Abe, and T. Otsuka, J. Phys.: Conf. Ser. **569**, 012063 (2014).
[9] I. Shimodaya, R. Tamagaki, and H. Tanaka, Prog. Theor. Phys. **27**, 793 (1962).
[10] M. Sakai, I. Shimodaya, Y. Akaishi, J. Hiura, and H. Tanaka, Prog. Theor. Phys. Suppl. **56**, 32 (1974).
[11] H. Kamada, A. Nogga, W. Glöckle, E. Hiyama, M. Kamimura, K. Varga, Y. Suzuki, M. Viviani, A. Kievsky, S. Rosati, J. Carlson, S. C. Pieper, R. B. Wiringa, P. Navrátil, B. R. Barrett, N. Barnea, W. Leidemann, and G. Orlandini, Phys. Rev. C **64**, 044001 (2001).
[12] H. Bandō, S. Nagata, and Y. Yamamoto, Prog. Theor. Phys. **44**, 646 (1970).
[13] R. B. Wiringa, S. C. Pieper, J. Carlson, and V. R. Pandharipande, Phys. Rev. C **62**, 014001 (2000).
[14] Y. Yamamoto, T. Togashi, and K. Katō, Prog. Theor. Phys. **124**, 315 (2010).
[15] Y. Kanada-En'yo, H. Horiuchi, and A. Ono, Phys. Rev. C **52**, 628 (1995).
[16] Y. Kanada-En'yo and H. Horiuchi, Phys. Rev. C **52**, 647 (1995).
[17] Y. Kanada-En'yo and H. Horiuchi, Prog. Theor. Phys. Suppl. **142**, 205 (2001).
[18] Y. Kanada-En'yo, M. Kimura, and A. Ono, Prog. Theor. Exp. Phys. **2012**, 01A202 (2012).
[19] T. Neff and H. Feldmeier, Nucl. Phys. A **738**, 357 (2004).
[20] R. Roth, T. Neff, and H. Feldmeier, Prog. Part. Nucl. Phys. **65**, 50 (2010).
[21] M. Chernykh, H. Feldmeier, T. Neff, P. von Neumann-Cosel, and A. Richter, Phys. Rev. Lett. **98**, 032501 (2007); **105**, 022501 (2010).
[22] A. Doté, Y. Kanada-En'yo, H. Horiuchi, Y. Akaishi, and K. Ikeda, Prog. Theor. Phys. **115**, 1069 (2006).
[23] N. Itagaki, H. Masui, M. Ito, and S. Aoyama, Phys. Rev. C **71**, 064307 (2005).
[24] H. Masui and N. Itagaki, Phys. Rev. C **75**, 054309 (2007).
[25] T. Yoshida, N. Itagaki, and T. Otsuka, Phys. Rev. C **79**, 034308 (2009).
[26] N. Itagaki, J. Cseh, and M. Płoszajczak, Phys. Rev. C **83**, 014302 (2011).
[27] T. Suhara, N. Itagaki, J. Cseh, and M. Płoszajczak, Phys. Rev. C **87**, 054334 (2013).
[28] T. Suhara and Y. Kanada-En'yo, Phys. Rev. C **91**, 024315 (2015).
[29] N. Itagaki, H. Matsuno, and T. Suhara, Prog. Theor. Exp. Phys. **2016**, 093D01 (2016).
[30] N. Itagaki, Phys. Rev. C **94**, 064324 (2016).
[31] H. Matsuno, N. Itagaki, T. Ichikawa, Y. Yoshida, and Y. Kanada-En'yo, Prog. Theor. Exp. Phys. **2017**, 063D01 (2017).
[32] H. Matsuno and N. Itagaki, Prog. Theor. Exp. Phys. **2017**, 123D05 (2017).
[33] N. Itagaki and A. Tohsaki, Phys. Rev. C **97**, 014307 (2018).
[34] T. Otsuka, T. Suzuki, R. Fujimoto, H. Grawe, and Y. Akaishi, Phys. Rev. Lett. **95**, 232502 (2005).
[35] N. Itagaki, H. Masui, M. Ito, S. Aoyama, and K. Ikeda, Phys. Rev. C **73**, 034310 (2006).
[36] T. Myo, K. Katō, and K. Ikeda, Prog. Theor. Phys. **113**, 763 (2005).
[37] T. Myo, S. Sugimoto, K. Katō, H. Toki, and K. Ikeda, Prog. Theor. Phys. **117**, 257 (2007).
[38] T. Myo, H. Toki, and K. Ikeda, Prog. Theor. Phys. **121**, 511 (2009).
[39] T. Myo, A. Umeya, H. Toki, and K. Ikeda, Phys. Rev. C **84**, 034315 (2011).
[40] T. Myo, A. Umeya, H. Toki, and K. Ikeda, Phys. Rev. C **86**, 024318 (2012).
[41] T. Myo, H. Toki, K. Ikeda, H. Horiuchi, and T. Suhara, Prog. Theor. Exp. Phys. **2015**, 073D02 (2015).
[42] T. Myo, H. Toki, K. Ikeda, H. Horiuchi, and T. Suhara, Phys. Lett. B **769**, 213 (2017).
[43] N. Itagaki and A. Tohsaki, Phys. Rev. C **97**, 014304 (2018).
[44] T. Myo, H. Toki, K. Ikeda, H. Horiuchi, T. Suhara, M. Lyu, M. Isaka, and T. Yamada, Prog. Theor. Exp. Phys. **2017**, 111D01 (2017).
[45] T. Myo, Prog. Theor. Exp. Phys. **2018**, 031D01 (2018).
[46] K. Horii, H. Toki, T. Myo, and K. Ikeda, Prog. Theor. Phys. **127**, 1019 (2012).
[47] A. B. Volkov, Nucl. Phys. **74**, 33 (1965).
[48] R. Tamagaki, Prog. Theor. Phys. **39**, 91 (1968).
[49] H. Furutani, H. Horiuchi, and R. Tamagaki, Prog. Theor. Phys. **62**, 981 (1979).
[50] L. Koester and W. Nistler, Z. Phys. A **272**, 189 (1975).
[51] G. F. de Téramond and B. Gabioud, Phys. Rev. C **36**, 691 (1987).
[52] I. Angeli and K. P. Marinova, At. Data Nucl. Data Tables **99**, 69 (2013).